Thin Solid Films 570 (2014) 123–128

Contents lists available at ScienceDirect

Thin Solid Films

journal homepage: www.elsevier.com/locate/tsf

Variable emissivity property of magnetron sputtering thermochromic film

Desong Fan [a], Qiang Li [a,*], Yimin Xuan [a,b], Ping Dai [a]

[a] School of Energy and Power Engineering, Nanjing University of Science and Technology, Nanjing, Jiangsu 210094, PR China
[b] College of Energy and Power Engineering, Nanjing University of Aeronautics and Astronautics, Nanjing, Jiangsu 210016, China

ARTICLE INFO

Article history:
Received 23 January 2014
Received in revised form 13 September 2014
Accepted 18 September 2014
Available online 28 September 2014

Keywords:
Manganite film
Variable emissivity
Thermal control

ABSTRACT

Thermochromic films are prepared on the substrate of yttria stabilized zirconia by radio frequency magnetron sputtering technique. Crystalline structure and surface morphology are characterized. Characterization result shows that the films are of perovskite structure exhibiting a dense and smooth surface morphology. Composition analysis is performed and the result indicated that the element composition of films can be adjusted to close its stoichiometric ratio by controlling the oxygen flow ratio. Temperature-dependent reflectivity and emissivity are studied. Reflectivity spectra show that the film undergoes a transition from a metallic state to a non-metallic state with increasing temperature. Emissivity of the films is large above the transition temperature and it decreases sharply below the temperature. The emissivity increment at 97–373 K can approach 0.39 by controlling sputtering pressure, working gas and film thickness.

1. Introduction

Manganese oxides $A_{1-x}B_xMnO_3$ (A = La, Sm, Pr, Nd; B is alkaline earth) are a typical thermochromic material which can change their thermal radiative properties with the variation of temperature. With this property, it is finding many applications in thermal furtivity and thermal control. For example, P. Laffez et al. [1–3] reported that Sm doped thermochromic material $Sm_{0.35}Ca_{0.65}MnO_3$ (SCMO) can be used as thermal furtivity coating because its emissivity decreases with increasing temperature. If a warm object coated SCMO appears on a cold background, it is difficult to be detected by the infrared camera in view of the weakened radiation sign from the object.

Another important application is the thermal control of miniature spacecraft, which has been reported in La doped thermochromic materials [4–8]. Contrary to the furtivity application, thermochromic materials for thermal control need a low emissivity at low temperature to maintain the heat, whereas at high temperature it is expected to have a high emissivity for dissipating the excess heat. If the material is fitted on the spacecraft surface, it can automatically control the emissive heat transfer from the spacecraft without assistance of any moving parts. Over the past years, many efforts on improving the applicability of the material have been carried out. Investigations from the Japan Aerospace Exploration Agency and Nippon Electric Company showed that the emissivity increment of two bulk materials $La_{0.825}Sr_{0.175}MnO_3$ and $La_{0.7}Ca_{0.3}MnO_3$ is 0.4 in a temperature range of 173–373 K [5–8]. Their results revealed that the material can be fabricated to a thin tile with a dimension of 40 × 40 × 0.2 mm^3 and a weight of 1.2 kg/m^2. We have also reported that the increment of normal emissivity is 0.5 at 173–373 K for the sample of Ca and Sr doping $La_{1-x}A_xMnO_3$ in our previous work [9]. The size of the sample is 40 mm × 40 mm with 400 μm thick and weight is 1.23 kg/m^2. J. Fang et al. [10] and J. Huang et al. [11] attempted to enhance the emissivity above T_p through introducing micro-structures or gratings on the material surface. In order to overcome the material drawback absorbing solar radiation, K. Shimazaki et al. [12,13] and D. Fan et al. [14,15] designed multi-layer optical structures on the material surface to reduce its solar absorptivity, and the reported solar absorptivity of the structured material can be reduced to 0.28. Moreover, the simulated experiment of space particles exposure revealed that the structured material possesses stabilized thermal radiative properties [5,16].

One can find these investigation efforts, which are mainly devoted to the performance of bulk material. Although the material can be fabricated into a ceramic tile with thickness in sub-millimeter dimensions to perform the temperature adjustment, it is still bulky or heavy in certain applications, especially in the spacecraft. In addition, it is also impossible to further reduce the thickness of bulk material in view of mechanical strength considerations. Meanwhile, the ceramic tile fabrication is inconvenient and low productive because of its low toughness. By comparison, thin film devices based on $La_{1-x}A_xMnO_3$ are more obvious to realize the weight reduction and there is no above-mentioned drawback. However, there exist only a few literatures to report the thermochromic film based on $La_{1-x}Sr_xMnO_3$. M. Soltani et al. [17] and D. Nikanpour et al. [18] prepared the $La_{1-x}Sr_xMnO_3$ ($x = 0.175$ and 0.3) thin films by reactive pulsed laser deposition method, but their emissivity variation remains modest. A. Boileau et al. [3]

* Corresponding author. Tel.: +86 25 84315488.
E-mail address: liqiang@mail.njust.edu.cn (Q. Li).

http://dx.doi.org/10.1016/j.tsf.2014.09.032
0040-6090/

synthesized SCMO thin films using dc reactive magnetron co-sputtering and indicated that SCMO films show a thermochromic effect over a wide wavelength range at room temperature. M.R. Ammar et al. [19] investigated the thermochromic behavior of SCMO pigment-polymer coating for thermochromic applications. The result shows that the optical transmittance of the coating exhibited a large variation between 173 K and 343 K in the wavelength range of 8–14 μm. C. Wu et al. [20] prepared the $La_{0.8}Sr_{0.2}MnO_3$ thin film by magnetron sputtering, whose emissivity increases from 0.53 at 173 K to 0.72 at 310 K. Obviously, the emissivity variation of these thin films is much smaller than that of their bulk counterparts. Therefore, further investigation will be required to access the bulk material properties in emissivity as much as possible.

In the work, the aim is to prepare the $La_{0.7}Sr_{0.3}MnO_3$ (LSMO) films on the substrate of yttria stabilized zirconia (YSZ) by magnetron sputtering technique, and investigate the variable emissivity properties of the films. Furthermore, some key parameters that influence the performance of the LSMO film, such as working gas, sputtering pressure and film thickness, are also discussed. The encouraging results have been obtained, which can provide fundamental data for developing a light-weight thermal control device for application in spacecraft.

2. Procedure for experiment

LSMO films were prepared on YSZ substrate by the radio frequency (RF) magnetron sputtering system (JGP800, Shenyang Scientific Instrument Co., China). The LSMO target used during sputtering was synthesized by the conventional solid-state reaction method using La_2O_3, $SrCO_3$ and MnO_2 powders as starting materials [9]. LSMO films were grown on YSZ (100) single crystal substrate at different sputtering pressures and different working gas, which is a mixture of argon containing different volume oxygen. An RF power of 90 W was used and the substrate temperature was kept at room temperature during deposition. The distance of between LSMO target and YSZ substrate is 50 mm. Other parameters in the experiment were listed in Table 1. In order to improve the oxygen content, the LSMO films were annealed ex-situ at 1073 K in flowing oxygen for 1 h. The film structure was characterized by X-ray diffraction (XRD, D8 ADVANCE, Bruker Co., Germany) using a Cu Kα ($\lambda_{Cu} = 1.5406$ Å) radiation source at 40 kV and 30 mA. The scanning was performed from 20 to 80° with steps of 0.05°. Microstructure of the film was analyzed by field emission scanning electron microscopy (SEM, S-4800, Hitachi Co., Japan) using an accelerating voltage of 15 kV. Composition analysis was performed in the SEM at an acceleration voltage of 20 kV and magnification of 1290 times by the energy dispersive X-ray spectroscopy (EDS, Thermo Electron Co., USA) with Noran System Six evaluation software and silicon drift detector. The film's thickness was also determined by cross-sectional SEM images with accelerated voltage of 20 kV. Surface roughness of the film was measured by the atomic force microscope (AFM, CSPM4000, Being Ltd., Beijing in China). The lateral resolution of the AFM is 0.26 nm and the vertical one is 0.1 nm. Infrared emissivity ϵ(T) determining thermal radiative properties of film was derived from reflectivity spectra according to ECSS-Q-70-09 [21], as expressed by

$$\epsilon(T) = \frac{\int_{2.5}^{25} [1-\rho(\lambda,T)]E_{\lambda,b}(\lambda,T)d\lambda}{\int_{2.5}^{25} E_{\lambda,b}(\lambda,T)d\lambda} \quad (1)$$

where $E_{\lambda,b}(\lambda,T)$ is blackbody radiative intensity. Temperature-dependent reflectivity $\rho(\lambda,T)$ can be measured by an accessory of Transmission-Reflection Dewar (catalog no. DER-300, Harrick Scientific Products, Inc., America) mounting on the Fourier transform infrared spectrometer (FT-IR, VERTEX 80 v, Bruker Co., Germany). The measured wavelength and temperature ranges are 2.5–25 μm and 97–373 K, respectively. A gold film was employed as a reference mirror to determine the reflectivity.

Table 1
Deposition condition and characteristics of LSMO films.

Sample	P (Pa)	GFR (%)	t (min)	La:Sr:Mn atom ratio	ARS (nm)	FT (μm)	ϵ_l	ϵ_h	Δϵ
LSMO1	0.8	0	170	0.85:0.13:1	0.60	0.90	0.28	0.52	0.24
LSMO2	0.8	20	180	0.71:0.12:1	0.60	0.90	0.24	0.62	0.38
LSMO3	0.8	33	195	0.71:0.14:1	0.64	0.89	0.27	0.67	0.40
LSMO4	0.8	50	215	0.61:0.22:1	0.66	0.90	0.27	0.67	0.40
LSMO5	0.5	20	173	0.71:0.12:1	0.71	0.91	0.22	0.56	0.34
LSMO6	1.2	20	182	0.66:0.15:1	0.69	0.89	0.15	0.52	0.37
LSMO7	2.0	20	198	0.66:0.29:1	0.65	0.90	0.17	0.56	0.39
LSMO8	0.8	20	150	0.71:0.13:1	0.53	0.76	0.53	0.55	0.02
LSMO9	0.8	20	240	0.69:0.13:1	0.75	1.19	0.28	0.67	0.39
LSMO10	0.8	20	300	0.70:0.12:1	0.90	1.49	0.29	0.65	0.36

P: sputtering pressure, GFR: gas flow ratio of O_2 / (O_2 + Ar), *t*: sputtering time, ARS: average roughness, FT: film thickness.

3. Results and discussion

XRD detection was performed to determine if desired crystalline structures were obtained under the designed conditions, where LSMO films have been annealed and corresponding bulk target is the as-prepared specimen by solid state reaction. Fig. 1 shows the XRD patterns of four LSMO films and one bulk target. The bottom pattern is the $La_{0.7}Sr_{0.3}MnO_3$ JCPDS card (no. 51-0409). All diffraction peaks match well with that of bulk target and films. It is clear that our bulk target contains split peaks at 32.9°, 40.6°, 58.6°, 68.9°, and 78°, where corresponding films only exhibit a single peak. This perhaps is induced by the preferable orientation of particles in films. It is noted that bulk target and LSMO films are single perovskite phase with rhombohedral structure. In addition, YSZ peaks can be observed in LSMO3 and LSMO8 films as marked by symbol □, which is related to their minimum film thickness (See Table 1).

Fig. 2 shows the SEM microstructure of thermochromic film. No matter how they are seen from the surface morphology of Fig. 2(a) or the cross-sectional micrograph of Fig. 2(b), it is still dense, crack-free, and uniform.

Sputtering pressure and working gas are two important factors to influence the performance of LSMO film. Therefore, they are taken into account in this study as follows. The effect of sputtering pressure and working gas on the roughness and composition of LSMO films are

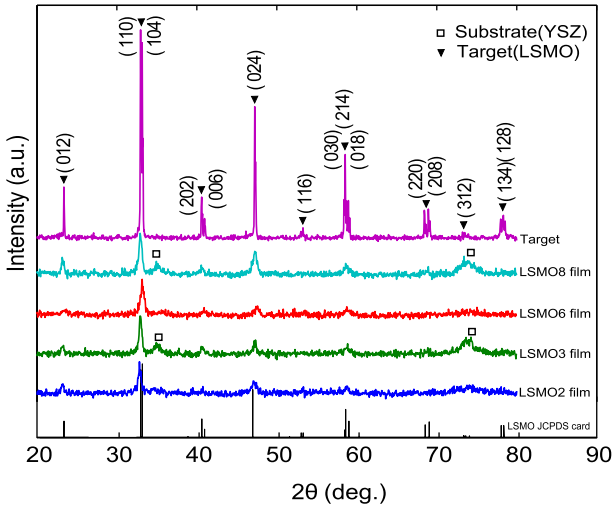

Fig. 1. XRD patterns of LSMO target and LSMO film.

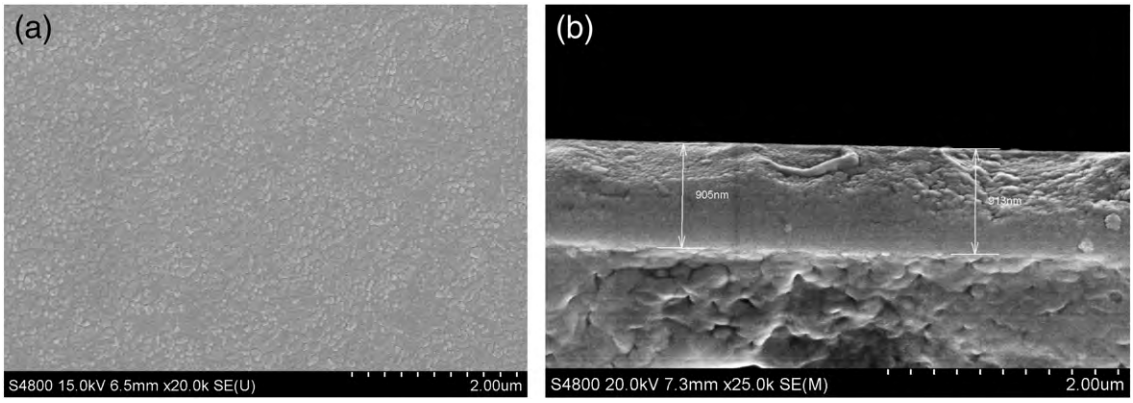

Fig. 2. SEM micrographs of (a) LSMO2 film surface and (b) LSMO5 film cross-section.

listed in Table 1. The thickness of LSMO films is also listed to be an average value of multiple measurements from the cross section SEM morphology. For example, LSMO5 film thickness is determined to be 0.91 μm as shown in Fig. 2(b). The roughness of films is determined by the AFM. For instance, the average roughness and root mean square roughness of LSMO2 film, which is estimated from Fig. 3 with 10 μm × 10 μm areas and 512 × 512 pixels, is 0.6 nm and 0.81 nm, respectively.

Under the same sputtering pressure condition, the film roughness scarcely shows any change with the increase of gas flow ratio O_2 / (O_2 + Ar) from 0% to 50%. Similarly, the change of film roughness is small when the sputtering pressure increases from 0.5 Pa to 2.0 Pa keeping the film thickness at 0.90 μm and working gas flow ratio for 20%. The results show that the effect of sputtering pressure and working gas on the film roughness is small enough. Moreover, when the sputtering pressure and the flow ratio of working gas are respectively set to 0.8 Pa and 20%, film roughness increases from 0.53 nm for the 0.76 μm thick sample to 0.90 nm for the 1.49 μm thick sample. The relationship between the film roughness and film thickness can be attributed to the film growth mode [22]. The growth mode of LSMO film on unheated YSZ substrate should be seen as Volmer–Weber type. In this mode, an island-like structure (see Fig. 3) is formed after an initial nucleation and it becomes large with the increase of film thickness, which in turn increases the film roughness.

Composition analysis in Table 1 checked by EDX shows that the LSMO target and LSMO films have a comparable stoichiometry. It can be observed that the La content is close to a stoichiometric ratio and Sr shows a lower concentration under the low sputtering pressure and low flow ratio. As the working gas is only argon, a notable difference between the result of composition analysis and the stoichiometric ratio can be found, i.e., an excess La content and a deficient Sr or Mn content in the composition analysis. When the gas flow ratio of O_2 / (O_2 + Ar) increases to 20% or 33%, the element composition of film is closer to the stoichiometric ratio. However, the La content is deficient in the case of film with the gas flow ratio approaching 50%. This means that the element composition of film can be adjusted by increasing the gas flow ratio of O_2 / (O_2 + Ar). This occurs because the oxygen content increases, which in turn increases its collision with the sputtered atoms during the sputtering process. Among the sputtered atoms, the mass of La atom is the largest. This implies that the energy loss of La atom is larger than that of Sr or Mn in the process of collision. Therefore, the La atom which arrived at the substrate is smaller than other atoms with the increase of the flow ratio O_2 / (O_2 + Ar). In addition, the influence of film thickness on the element composition of the film is unobvious.

Fig. 4 shows the measured reflectivity of LSMO film in the temperature range of 97–373 K. It is noted that the reflectivity of film decreases with increasing temperature below 313 K and remains almost constant

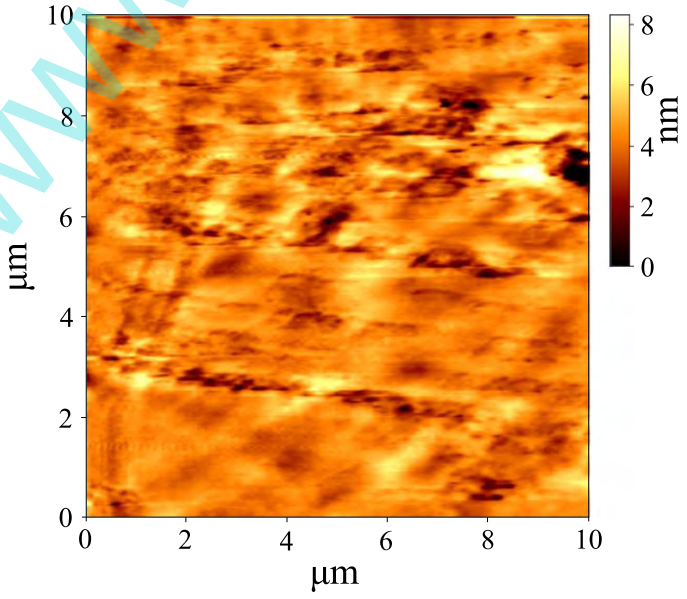

Fig. 3. AFM patterns of LSMO2 film.

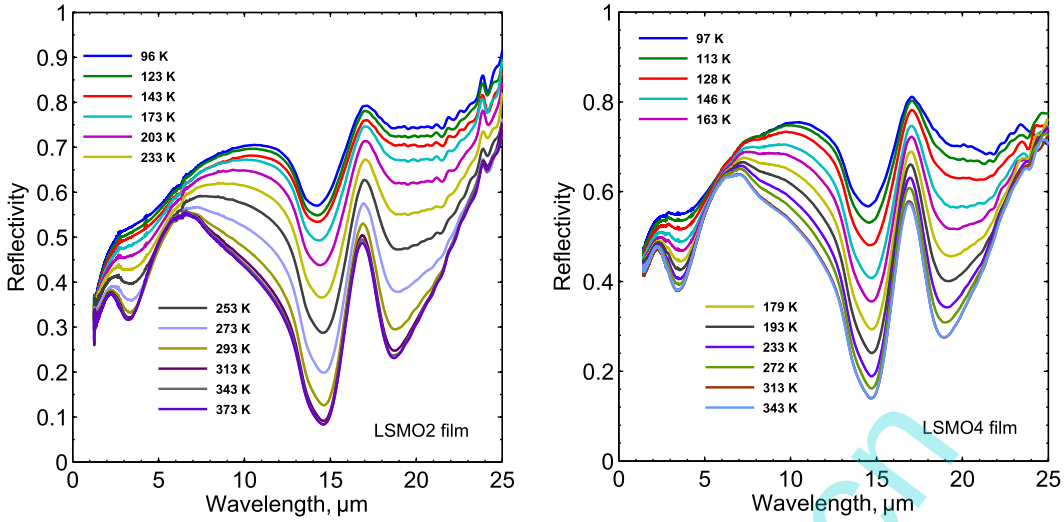

Fig. 4. Variation of the reflectivity of LSMO film with temperature.

with the increase of temperature above 313 K. A sharp infrared peak at the wavelength of 17 μm under a different test temperature can be observed, which dues to the transverse optical phonons. In theory, there are three strong transverse optical phonon peaks in perovskite sample [23–25]. The other two phonon peaks occur at 30 μm and 60 μm, corresponding to Mn–O–Mn bending mode, and La-site external mode, respectively. In view of the limited spectral range of spectrometer, we only observed the optical phonon peak corresponding to Mn–O stretching vibration in our samples. The phonon peak toward the low temperature 97 K is still sharp comparing with that of LSMO bulk material, which has been reported in the previous works [9,25]. The fact suggests that LSMO film is "more nonmetallic" than its bulk counterpart at low temperature zones. For the LSMO bulk material, the lower temperature is, the smoother peak at 17 μm becomes. The phenomenon has been explained by a dielectric screening effect [23,26]. Namely, the electron activity in bulk material is heightened under a lower temperature. Therefore, it is considered that the contribution of optical phonon in LSMO film is still dominant under the lower temperature, which leads to LSMO film exhibiting more nonmetallic features. The sharp peaks under low temperature zones seem to be common in manganite film as reported by these authors [4,27]. With the increase of temperature, a broad peak appearing around 6 μm in our films. Similar feature has been observed by previous authors in both single crystalline [28] and thin film manganites [4,29,30]. H. Lee et al. [28] suggested that the broad peak appearing in $Nd_{0.7}Sr_{0.3}MnO_3$ single crystal comes from the optical transitions between electronic levels. And, C. Hartinger et al. [29] reported that the broad peak is related to the large polaron excitation in $La_{2/3}Sr_{1/3}MnO_3$ thin film.

Infrared emissivity of LSMO films are obtained by integrating the reflectivity spectra of films [15]. The results are shown in Figs. 5–8. It can be seen from these figures that the LSMO films exhibit thermochromic properties, of which their emissivities are small at lower temperature but large at a higher temperature. The emissivity variation has been listed in Table 1.

Comparisons are given for the emissivity of LSMO target and LSMO2 film in Fig. 5. For the substrate, its emissivity remains constant with the increase of temperature. However, the film and target show a significant emissivity variation upon heating. It is noticed that the emissivity of the target is lower than that of the film in the whole temperature range owing to the multiple reflection in film sample. Transition temperature, which can be approximately determined from the turning point of temperature dependent emissivity, is about 273 K for LSMO target and LSMO2 film. The metal-insulator transition temperature of LSMO target is much lower than that of numerous literature results (about 350 K) [31,32]. The reason may be related to the oxygen deficiency. According to the double exchange theory, the occurrence of oxygen deficiency could break the hopping of electrons in addition to decreasing the density of charge carriers, which leads to a lower metal-insulator transition.

It can be found that from Fig. 5, the transition temperature of films are low even though it has been post-annealed. This results are consistent with that of literatures [33,20,30]. S. Jiang et al. [30] reported that the transition temperature of LSMO film after annealing is only 168 K, while it can be adjusted to 267 K by 50 KeV oxygen ion implantation. D. Sahu et al. [33] indicated that the transition temperature of as-grown LSMO films can be enhanced significantly up to 270 K by annealing at 1273 K. Indeed, as already observed in manganite films, the transition temperature is strongly affected by the oxygen content. Besides the oxygen content, it is reported that the metal-insulator transition can be driven by many physical mechanisms such as poor electrical connection between grains [34], non-stoichiometric composition [35], strain effect and interstitial oxygen incorporation [36,37]. The low transition temperature of LSMO film in our experiment cannot be described to unique mechanisms. The apparent influences of oxygen

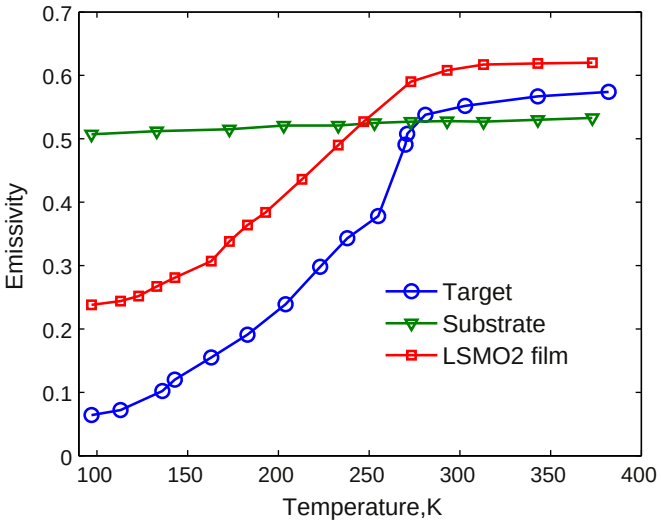

Fig. 5. Emissivity of LSMO target and LSMO2 films.

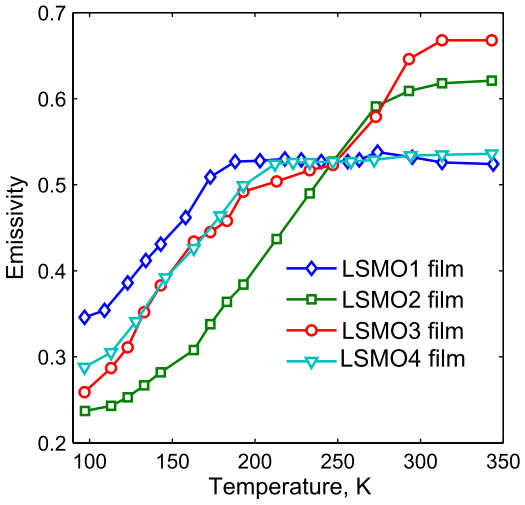

Fig. 6. Emissivity of LSMO film at different flow ratio of O_2 / (O_2 + Ar).

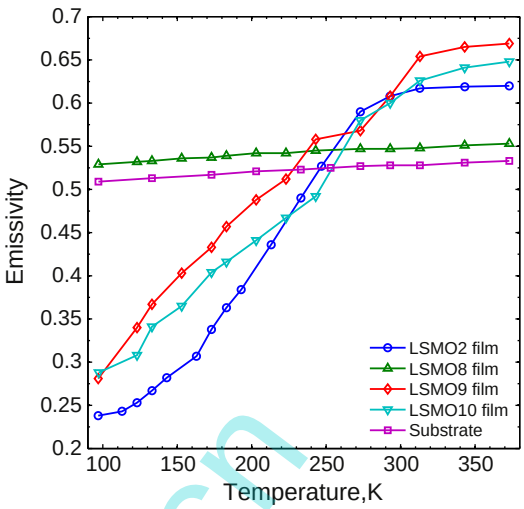

Fig. 8. Emissivity of LSMO film at different film thickness.

flow ratio, sputtering pressure, and film thickness will be discussed in a later section.

The influence of the O_2 / (O_2 + Ar) flow ratio on the emissivity of film are shown in Fig. 6. The sputtering pressure of LSMO1 to LSMO4 film is fixed to 0.8 Pa and their O_2 / (O_2 + Ar) flow ratios is 0%, 20%, 33% and 50%, respectively. The emissivity increment of film increases with the O_2 / (O_2 + Ar) flow ratio below 33% and then becomes small at 50%. This is revealed that LSMO films have reduced oxygen deficiencies with increasing oxygen flow during deposition. The reduced oxygen contents in films leads to hole doping through an enhancement of Mn^{4+}/Mn^{3+} ratio, which would explain why transition temperature increase [33]. The higher the temperature, the larger emissivity increment becomes. Thus, the continued increase of oxygen content leads to an increase of La site deficient in LSMO film resulting in non-stoichiometry as discussed above. Therefore, the emissivity transition of LSMO4 film with oxygen flow ratio of 50% occurs at a relatively low temperature at about 213 K.

The emissivity of LSMO film at different sputtering pressure is given in Fig. 7. The sputtering pressure is 0.5 Pa, 0.8 Pa, 1.2 Pa and 2.0 Pa for the sample LSMO5, LSMO2, LSMO6 and LSMO7, respectively. It is seen that the emissivity transition seems to occur at a relative higher temperature with sputtering pressure increasing. Film growth in a low pressure environment contains high densities of defects and oxygen deficiency due to less oxygen content. With the increase of pressure, the oxygen

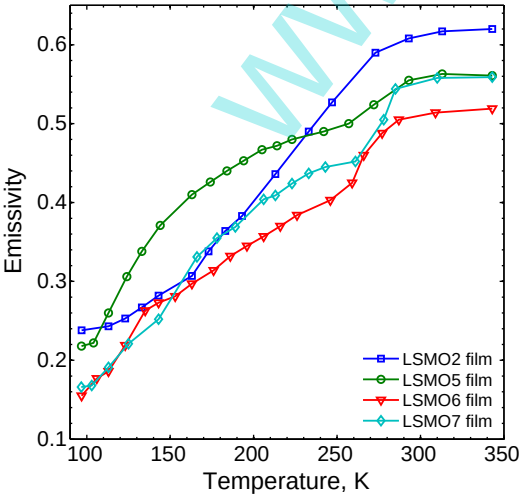

Fig. 7. Emissivity of LSMO film at different sputtering pressure.

content increases, which enhances the transition temperature [38]. Moreover, the influence of sputtering pressure on LSMO emissivity may be due to interface problems and change in the strain effect between the film and substrate. Other possibilities may be existing but it is still unclear in our experimental results. The emissivity increment as listed Table 1 in the whole temperature range exhibits a slight rise with the increase of sputtering pressure.

Fig. 8 shows the influence of film thickness on film emissivity. The sputtering pressure is kept at 0.8 Pa and the O_2 / (O_2 + Ar) flow ratio is set to 20%. The film thickness is 0.76 μm, 0.90 μm, 1.19 μm and 1.49 μm for the LSMO8, LSMO2, LSMO9 and LSMO10, respectively. It can be found that the film with thickness near or exceeding 0.89 μm shows a thermochromic property, whose emissivity increases with temperature. For example, the emissivity of LSMO9 and LSMO10 shows a quick rise below 273 K and the rise becomes slow above 273 K. However, the emissivity of film almost does not change with increasing temperature when the film thickness is less than 0.89 μm, like the LSMO8 sample, $\Delta\epsilon = 0.02$. In fact, a proper film thickness is important for a variable emissivity device because the infrared radiation of a material is mostly determined by the thin layer of material surface (i.e., skin depth). If the film thickness is slightly larger than that of the skin depth, the infrared properties of the film is comparable to that of its bulk counterpart. Conversely, it is subjected to the substrate. As shown in Fig. 8, the film thickness of LSMO8 sample is thinner than its skin depth (300–800 nm), which have been reported by Y. Shimakawa et al. [4]. Consequently its infrared radiation includes the reflected infrared radiation from the YSZ substrate. The high emissivity property of YSZ leads to a high emissivity for the film sample even at a low temperature resulting in an inconspicuous emissivity variation. Therefore, it is necessary to ensure a proper LSMO film thickness to maintain the emissivity variation of device.

4. Conclusion

LSMO films were prepared on YSZ substrate by the RF magnetron sputtering technique. Surface morphology indicated that the film is dense and smooth. XRD analysis showed that the film exhibits the characteristics of a perovskite structure. The result of composition analysis suggested that the element composition of the film can be adjusted to close its stoichiometric ratio by regulating the O_2 / (O_2 + Ar) flow ratio. Reflectivity spectra showed that the film undergoes a transition from a metallic state to a non-metallic state and an intrinsic phonon structure at wavelength of 17 μm can be observed. The measured emissivity indicated that LSMO film exhibits a small emissivity value at lower temperature and a large emissivity value at higher temperature. The

influence factors on the film emissivity have been discussed. The emissivity increment of film can be arrived to 0.39 at 97–373 K by keeping the sputtering pressure for 0.8 Pa, the O_2 / (O_2 + Ar) flow ratio for 20% and film thickness exceeding 0.89 μm. The encouraging results can provide fundamental data for developing a lightweight thermal control device for application in spacecraft.

Acknowledgments

This work is sponsored by the National Science Foundation of China (grant nos. 51225602 and 51406086), the Natural Science Foundation of Jiangsu Province (no. BK20140783), and the 2014 Zijin Intelligent Program of Nanjing University of Science and Technology.

References

[1] P. Laffez, M. Zaghrioui, L. Reversat, P. Ruello, Electron doped $Sm_{1-x}Ca_xMnO_3$ perovskite manganite as potential infrared thermochromic switch, Appl. Phys. Lett. 89 (2006) 081909/1.
[2] P. Laffez, C. Napierala, M. Zaghrioui, V.T. Phuoc, A. Hassini, M.R. Ammar, Thermal emittance changes at the charge ordering transition of $Sm_{0.35}Ca_{0.65}MnO_3$, Appl. Phys. Lett. 93 (2008) 151910/1.
[3] A. Boileau, F. Capon, S. Barrat, P. Laffez, J. Pierson, Thermochromic effect at room temperature of $Sm_{0.5}Ca_{0.5}MnO_3$ thin films, J. Appl. Phys. 111 (2012) 113517/1.
[4] Y. Shimakawa, T. Yoshitake, Y. Kubo, T. Machida, K. Shinagawa, A. Okamoto, Y. Nakamura, A. Ochi, S. Tachikawa, A. Ohnishi, A variable-emittance radiator based on a metal-insulator transition of (La, Sr)MnO3 thin films, Appl. Phys. Lett. 80 (2002) 4864.
[5] S. Tachikawa, A. Ohnishi, Y. Shimakawa, A. Ochi, A. Okamoto, Y. Nakamura, Development of a variable emittance radiator based on a perovskite manganese oxide, J. Thermophys. Heat Transf. 17 (2003) 264.
[6] K. Shimazaki, S. Tachikawa, A. Ohnishi, Y. Nagasaka, Temperature dependence of total hemispherical emittance in perovskite-type manganese oxides, $La_{1-x}Sr_xMnO_3$, High Temp. High Pressure 33 (2001) 525.
[7] K. Shimazaki, S. Tachikawa, A. Ohnishi, Y. Nagasaka, Radiative and optical properties of $La_{1-x}Sr_xMnO_3$($0 < x < 0.4$) in the vicinity of metal-insulator transition temperatures from 173 to 413 K, Int. J. Thermophys. 22 (2001) 1549.
[8] A. Ochi, T. Mori, Y. Shimakawa, Y. Kubo, A. Okamoto, Y. Nakamura, S. Tachikawa, A. Ohnishi, K. Shimazaki, Variable thermal emittance radiator using metal-insulator phase transition in $La_{1-x}Sr_xMnO_3$, Jpn. J. Appl. Phys. 41 (2002) 7263.
[9] D. Fan, Q. Li, Y. Xuan, H. Tan, J. Fang, Temperature-dependent infrared properties of Ca doped (La, Sr)MnO3 compositions with potential thermal control application, Appl. Therm. Eng. 51 (2013) 255.
[10] J. Fang, Y. Xuan, Q. Li, D. Fan, J. Huang, Investigation on the coupling effect of thermochromism and microstructure on spectral properties of structured surfaces, Appl. Surf. Sci. 258 (2012) 7140.
[11] J. Huang, Y. Xuan, Q. Li, Perovskite-type oxide films combined with gratings for reduction of material consumption and improvement of thermochromism property, J. Quant. Spectrosc. Radiat. Transf. 112 (2011) 2592.
[12] K. Shimazaki, A. Ohnishi, Y. Nagasaka, Development of spectral selective multilayer film for a variable emittance device and its radiation properties measurements, Int. J. Thermophys. 24 (2003) 757.
[13] K. Shimazaki, A. Ohnishi, Y. Nagasaka, Computational design of solar reflection and far-infrared transmission films for a variable emittance device, Appl. Opt. 42 (2003) 1360.
[14] D. Fan, Q. Li, Y. Xuan, Tailoring the solar absorptivity of thermochromic material $La_{0.7}Ca_{0.2}Sr_{0.1}MnO_3$, J. Quant. Spectrosc. Radiat. Transf. 112 (2011) 2794.
[15] D. Fan, Q. Li, Y. Xuan, H. Tan, J. Fang, Radiative properties of thermochromic material with solar reflection films, Sol. Energy Mater. Sol. Cells 112 (2013) 52.
[16] D. Fan, Q. Li, Y. Xuan, H. Tan, Degradation of thermal radiative properties of variable emissivity device based on manganese oxides in simulated space environment, Int. J. Therm. Sci. 71 (2013) 258.
[17] M. Soltani, M. Chaker, X.X. Jiang, D. Nikanpour, J. Margot, Thermochromic $La_{1-x}Sr_xMnO_3$($x = 0.1$, 0.175, and 0.3) smart coatings grown by reactive pulsed laser deposition, J. Vac. Sci. Technol. A24 (2006) 1518.
[18] D. Nikanpour, X.X. Jiang, S. Genaron, G. Wang, An autonomous variable emittance thermal radiatior for small & microsat temperature control, 4th symposium of Small Satellites Systems and Services, ESA, Noordwijk,The Netherlands, 2008.
[19] M.R. Ammar, C. Napierala, P. Laffez, Infrared thermochromic behaviour of a composite $Sm_{0.65}Ca_{0.35}MnO_3$-poly(styrene-co-acrylonitrile) film, Smart Mater. Struct. 18 (2009) 055002.
[20] C. Wu, J. Qiu, J. Wang, M. Xu, L. Wang, Thermochromic property of $La_{0.8}Sr_{0.2}MnO_3$ thin-film material sputtered on quartz glass, J. Alloys Compd. 506 (2010) L22.
[21] ECSS-Q-70-09A, ESA space product assurance—measurements of thermo-optical properties of thermal control materials, 2003.
[22] Y. Sato, M. Taketomo, N. Ito, A. Miyamura, Y. Shigesato, Comparative study on early stages of film growth for transparent conductive oxide films deposited by dc magnetron sputtering, Thin Solid Films 516 (2008) 4598.
[23] Y. Okimoto, T. Katsufuji, T. Ishikawa, A. Urushibara, T. Arima, Y. Tokura, Anomalous variation of optical spectra with spin polarization in double-exchange ferromagnet $La_{1-x}Sr_xMnO_3$, Phys. Rev. Lett. 75 (1995) 109.
[24] K.H. Kim, J.Y. Gu, H.S. Choi, G.W. Park, T.W. Noh, Frequency shifts of the internal phonon modes in $La_{0.7}Ca_{0.3}MnO_3$, Phys. Rev. Lett. 77 (1996) 1877.
[25] Y. Okimoto, T. Katsufuji, T. Ishikawa, T. Arima, Y. Tokura, Variation of electronic structure in $La_{1-x}Sr_xMnO_3$, ($0 < x < 0.3$) as investigated by optical conductivity spectra, Phys. Rev. B 55 (1997) 4206.
[26] G.D. Marzi, Z.V. Popović, A. Cantarero, Z. Dohcević-Mitrović, N. Paunović, J. Bok, F. Sapiña, Effect of a-site and b-site substitution on the infrared reflectivity spectra of $La_{1-y}A_yMn_{1-x}B_xO_3$(A = Ba, Sr; B = Cu, Zn, Sc; $0 < y \leq 0.3$;$0 \leq x \leq 0.1$) manganites, Phys. Rev. B 68 (2003) 064302.
[27] Q. Li, D. Fan, Y. Xuan, Thermal radiative properties of plasma sprayed thermochromic coating, J. Alloys Compd. 583 (2014) 516.
[28] H. Lee, J. Jung, Y. Lee, J. Ahn, T. Noh, K. Kim, S. Cheong, Optical properties of a $Nd_{0.7}Sr_{0.3}MnO_3$ single crystal, Phys. Rev. B 60 (1999) 5251.
[29] C. Hartinger, F. Mayr, J. Deisenhofer, A. Loidl, T. Kopp, Large and small polaron excitations in $La_{2/3}(Sr/Ca)_{1/3}MnO_3$ films, Phys. Rev. B 69 (2004) 100403.
[30] S. Jiang, X. Ma, G. Wang, G. Tang, Z. Wang, Z. Zhou, Characteristics of $La_{0.7}Sr_{0.3}MnO_{3-\delta}$ films treated by oxygen plasma immersion ion implantation, Surf. Coat. Technol. 229 (2013) 76.
[31] K. Ghosh, C.J. Lobb, R.L. Greene, S.G. Karabashev, D.A. Shulyatev, A.A. Arsenov, Y. Mukovskii, Critical phenomena in the double-exchange ferromagnet $La_{0.7}Sr_{0.3}MnO_3$, Phys. Rev. Lett. 81 (1998) 4740.
[32] Y. Tomioka, A. Asamitsu, Y. Tokura, Magnetotransport properties and magnetostructural phenomenon in single crystals of $La_{0.7}(Ca_{1-y}Sr_y)_{0.3}MnO_3$, Phys. Rev. B 63 (2000) 024421/1.
[33] D. Sahu, D. Mishra, J.-L. Huang, B. Roul, Annealing effect on the properties of $La_{0.7}Sr_{0.3}MnO_3$ thin film grown on Si substrates by DC sputtering, Phys. B Condens. Matter 396 (2007) 75.
[34] G. Ren, S. Yuan, Z. Tian, Electrical transport and magnetoresistance in $La_{2/3}Sr_{1/3}MnO_3$ polycrystalline composite thin films, Thin Solid Films 517 (2009) 3748.
[35] J. Sun, H. Yeung, H. Wong, T. Zhu, B. Shen, Effects of vacuum annealing on the transport property of $La_{0.67}Sr_{0.33}MnO_3$ films, Eur. Phys. J. B. 35 (2003) 481.
[36] B. Li, F. Tian, L. Yang, X. Wang, H. Zhu, T. Endo, Strain effects and phase separation tendency in highly strained $La_{0.7}Ba_{0.3}MnO_3$ thin films on $LaAlO_3$ substrates, Thin Solid Films 519 (2011) 2381.
[37] S. Valencia, L. Balcells, J. Fontcuberta, B. Martínez, Strain-induced charge depletion in $La_{2/3}Ca_{1/3}MnO_3$ epitaxial thin films, Appl. Phys. Lett. 82 (2003) 4531.
[38] D. Sahu, $La_{0.7S}SR_{0.3}MnO_3$ film prepared by dc sputtering on silicon substrate: effect of working pressure, J. Phys. Chem. Solids 73 (2012) 622.